Construction and Building Materials xxx (xxxx) 146485

Contents lists available at ScienceDirect

Construction and Building Materials

journal homepage: www.elsevier.com/locate/conbuildmat

Load-bearing performance of corroded reinforced concrete pipes rehabilitated with CIPP liners: Full-scale tests and a design-oriented bearing capacity model

Jing Liu [a], Wenwen Du [a], Chang Ma [a], Jingguo Cao [b, 1, *], Kangfu Sun [b, c, 2, **]

[a] College of Marine and Environmental Sciences, Tianjin University of Science & Technology, Tianjin 300457, China
[b] College of Chemical Engineering and Materials Science, Tianjin University of Science & Technology, Tianjin 300457, China
[c] Ningbo Water Meter (Group) Co., Ltd., Ningbo 315000, China

ARTICLE INFO

Keywords:
Reinforced concrete pipes (RCPs)
CIPP lining
Three-edge bearing test (TEBT)
Residual load-bearing capacity
Numerical simulation

ABSTRACT

Reinforced concrete pipes (RCPs) are prone to structural deterioration during long-term service due to internal corrosion, resulting in reduced load-bearing capacity. Cured-in-place pipe (CIPP) lining is a widely used trenchless rehabilitation technique; however, the quantitative relationship between liner thickness and structural enhancement remains insufficiently understood. In this study, full-scale three-edge bearing tests (TEBT) and three-dimensional finite element analyses were conducted on intact and corroded RCPs rehabilitated with CIPP liners of different thicknesses. The results show that corrosion reduces the cracking and ultimate loads of RCPs, whereas CIPP rehabilitation significantly enhances structural capacity, with increases of approximately 11–30% and 2–44%, respectively. This study reveals that corrosion preserves the intrinsic cracking–ultimate load relationship while reducing structural resistance, indicating that corrosion affects load capacity magnitude without altering the underlying structural response mechanism. Numerical predictions agree well with experimental results, and a design-oriented bearing capacity modification model is developed within the framework of Zhu's plastic-hinge theory. By introducing a correction factor of K = 1.12, the prediction error is reduced to within approximately 2%, demonstrating the accuracy and engineering applicability of the proposed model.

1. Introduction

Urban underground pipeline networks are critical infrastructure systems that are continuously exposed to chemical corrosion, microbial attack, traffic loading, and ground deformation. As a result, reinforced concrete drainage pipes (RCPs) are prone to deterioration such as internal surface corrosion, crack propagation, and joint dislocation, leading to progressive degradation of circumferential stiffness and overall load-bearing performance [1,2]. Under complex service conditions involving uneven ground settlement, fault movement, and variations in soil cover, the residual load-bearing capacity has therefore become a key indicator for evaluating pipeline structural safety [3–6].

Cured-in-place pipe (CIPP) lining has been widely applied in drainage pipeline rehabilitation due to its construction convenience and strong adaptability. By forming a glass fiber reinforced polymer (GFRP) strengthening layer inside the host pipe, CIPP transforms the RCP into a composite structure, thereby enhancing its stiffness and load-bearing capacity [7–10]. Existing studies have shown that the strengthening effect is highly sensitive to liner thickness [11]. However, current design standards and guidelines, such as ASTM F1216, DWA-A 143–2, and AWWA M28, are largely based on empirical formulations or single-material assumptions, and thus fail to adequately reflect thickness–modulus matching, interface interaction, and corrosion-induced degradation in RCP-CIPP composite systems [12–14].

* Corresponding author.
** Corresponding author at: College of Chemical Engineering and Materials Science, Tianjin University of Science & Technology, Tianjin 300457, China.
E-mail addresses: cjg@tust.edu.cn (J. Cao), skf@tust.edu.cn (K. Sun).
[1] Permanent address: No.9, Thirteenth Street, Binhai New Area Economic and Technological Development Zone, Tianjin, Tianjin University of Science & Technology, Tianjin, 300457, China.
[2] Permanent address: No.9, Thirteenth Street, Binhai New Area Economic and Technological Development Zone, Tianjin, Tianjin University of Science & Technology, Tianjin, 300457, China.

https://doi.org/10.1016/j.conbuildmat.2026.146485
Received 19 December 2025; Received in revised form 2 April 2026; Accepted 24 April 2026
0950-0618/

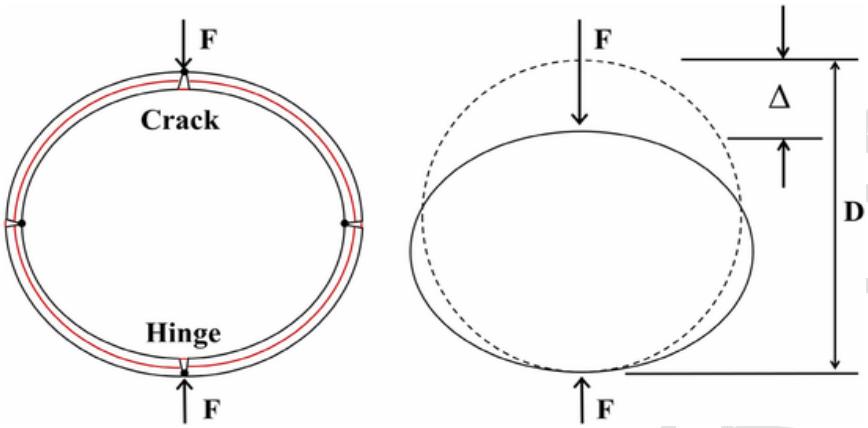

Fig. 1. Free-body diagram of a ring structure subjected to a concentrated load F.

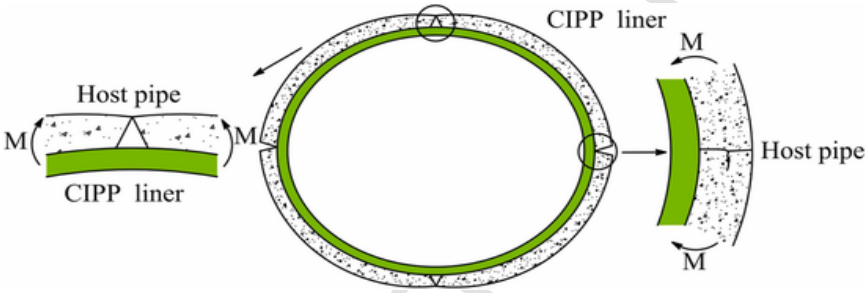

Fig. 2. Load transfer mechanism of the composite structure formed by the CIPP liner and the host pipe.

Table 1
Test conditions of pipe specimens.

Group	Corrosion depth(mm)	length (mm)	Wall thickness (mm)	Liner thickness (mm)	Repair type	Remarks
S1	0	2500	80	0	RCP	Reference specimen
S2	0	2500	80	12	Fully structural	UV-CIPP liner
S3	60	2500	80	0	Corroded RCP	Corrosion simulated by milling
S4	60	2500	80	12	Fully structural	Corroded + liner

Table 2
Summary of experimental results (mean and standard deviation).

Group	Cracking load (kN)	Ultimate load (kN)
S1	187 ± 27.83 kN	265 ± 45.08 kN
S2	234.77 ± 25.16 kN	293.55 ± 11.69 kN
S3	146.58 ± 25.05 kN	225.07 ± 13.31 kN
S4	176.69 ± 5.59 kN	265.80 ± 10.65 kN

Note: Each value represents the mean and standard deviation obtained from three parallel specimens for each test condition.

In recent years, multi-scale investigations combining TEBT, distributed optical fiber sensing, and finite element modeling (FEM) have provided deeper insights into the mechanical behavior of composite pipe structures. Wang et al. [15], Dong [16], Zhai et al. [17], and Wang et al. [18] systematically investigated the effects of liner thickness, pipe geometry, and interface conditions on stiffness distribution, load transfer, and bending response of CIPP-rehabilitated pipes through TEBT and numerical analyses. Based on experimental observations, Wang et al. [19] further proposed a bearing capacity model for concrete pipe–CIPP composite systems, indicating that the required CIPP thickness could be reduced compared with ASTM-based designs [20,21].

Although the ASTM C497 TEBT method [22], the ASTM F1216 CIPP design approach, and the AWWA M28 rehabilitation guideline [23] provide useful references for pipeline structural assessment, they generally neglect the effects of interface interaction, liner thickness variation, and corrosion-induced degradation in RCP-CIPP composite systems, which limits their ability to accurately predict structural performance under realistic engineering conditions.

Previous studies on the structural performance of CIPP-rehabilitated pipelines have primarily focused on intact host pipes or relied heavily on numerical simulations [24–26]. Experimental investigations are often limited to small-scale specimens or simplified loading conditions, and the coupled effects of corrosion-induced degradation and liner thickness variation remain insufficiently explored. Moreover, most existing analytical and design-oriented models are developed for intact pipes and do not explicitly account for the influence of corrosion damage on load-bearing mechanisms. As a result, the applicability of current approaches for assessing deteriorated RCP-CIPP composite systems under realistic service conditions is limited.

To address these limitations, the present study integrates full-scale TEBT with three-dimensional finite element analyses to systematically investigate the structural behavior of both intact and corroded RCPs rehabilitated with CIPP liners. Emphasis is placed on the role of corrosion-induced degradation in governing failure mode evolution, strain response, and load-bearing performance before and after rehabilitation. Furthermore, based on Zhu's plastic-hinge model, a design-oriented bearing capacity modification method is proposed by incorporating

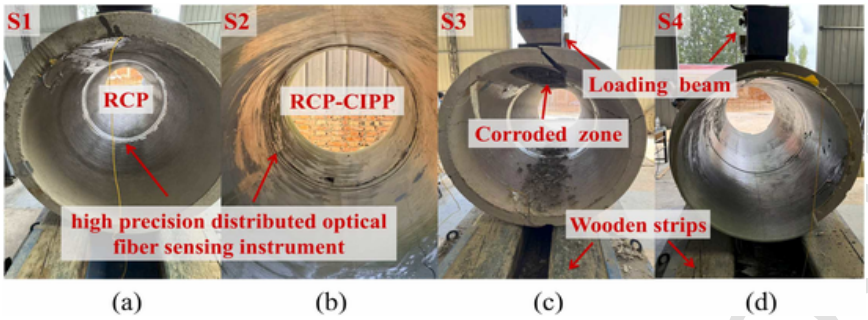

Fig. 3. Specimens and loading setup: (a) intact RCP; (b) RCP-CIPP; (c) corroded RCP; (d) corroded RCP-CIPP.

Fig. 4. Photograph of the TEBT experimental setup.

both liner thickness effects and corrosion-induced strength reduction, thereby extending existing bearing capacity models toward practical rehabilitation design.

2. Bearing capacity calculations for RCP and RCP-CIPP composite pipes

Existing plastic-hinge-based formulations for intact and corroded RCPs under TEBT loading are first reviewed. Building on the framework proposed by Zhu et al. , the model is further extended to RCP-CIPP composite pipes by explicitly accounting for the structural contribution of the CIPP liner, including stiffness and thickness effects.

2.1. Overview of the Zhu model

(1) Bearing capacity of intact RCPs

Reynolds et al. [28] proposed distinct failure modes for rigid and flexible pipes, as illustrated in Fig. 1. Rigid pipes exhibit limited deformation and primarily resist loads through their structural strength, whereas flexible pipes undergo significant deformation and rely on soil structure interaction to redistribute external loads.

For intact RCPs, the bearing capacity is evaluated using the three-edge bearing (TEB) method based on the plastic-hinge failure mechanism of rigid pipes. According to the model proposed by Zhu et al. [29],

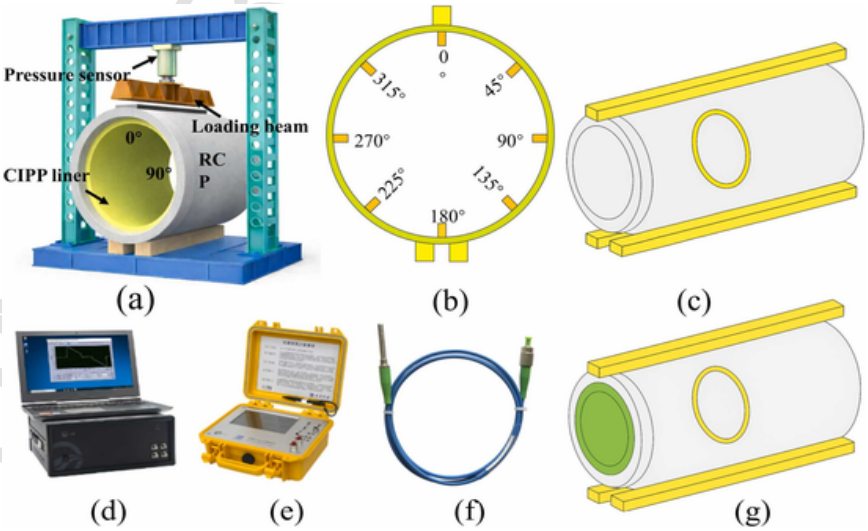

Fig. 5. Schematic diagram of testing equipment and sensor layout: (a) testing apparatus; (b) circumferential angle identification on the inner wall; (c) optical fiber layout in the RCP; (d) optical frequency domain reflectometry(OFDR)-based distributed optical fiber sensing system; (e) distributed optical fiber interrogation unit; (f) fiber Bragg grating(FBG) optical fiber strain sensor; and (g) optical fiber layout in the CIPP liner.

Table 3
Material properties used in the numerical simulations.

Part	Density (kg/m³)	Elastic modulus (MPa)	Poisson's ratio	Source
Concrete	2400	33,500	0.3	Ref. [36]
Steel	7850	210,000	0.3	Ref. [37]
Rubber pad	1000	10	0.3	Ref. [38]
Timber beam	900	10,000	0.3	Ref. [39]
CIPP liner	1800	14,360	0.3	Experimental measurement

Table 4
Mechanical properties of the CIPP liner used in the numerical model.

Property	Value	Unit	Test standard
thickness	12	mm	Determination of Dimensions of Plastic Components for Plastic Pipeline Systems GB/T8806
Tensile strength	147.64	MPa	Determination of Tensile Properties of Plastics-Part 4: Test Conditions for Isotropic and Orthotropic Fiber-Reinforced Composites GB/T 1040.4
Flexural strength	158.88	MPa	Test Method for Flexural Properties of Fiber-Reinforced Plastics GB/T 1449
Flexural modulus	14360	MPa	

plastic hinges form at the crown, invert, and springlines, allowing the pipe ring to be idealized as a closed system composed of four rigid segments. Based on this failure mechanism, the ultimate bearing capacity is derived using an energy balance approach, which is subsequently extended in this study to RCP-CIPP composite pipes, i.e.,

$$F = \frac{M_{crown}}{R} + \frac{M_{invert}}{R} + 2\frac{M_{spring}}{R} \tag{1}$$

Where F is the ultimate bearing capacity under TEB loading(kN); M_{crown}, M_{invert}, and M_{spring} denote the plastic bending moments at the crown, invert, and springlines, respectively(kN·m); and R is the mean radius to the centroid of the pipe wall cross-section(m). Owing to geometric and reinforcement symmetry, Eq. (1) can be simplified as:

$$F = 2\left(\frac{M_v}{R} + \frac{M_h}{R}\right) \tag{2}$$

The load-bearing capacity of the vertical section is mainly provided by tensile resistance of the outer reinforcement cage and the combined contribution of the inner reinforcement cage and the concrete compression zone, which can be expressed as:

$$M_v = \sigma_{vo}A'_s a'_s + \sigma_{vi}A_s\left(h - a_s\right) \tag{3}$$

The plastic bending moment of the horizontal section is given by:

$$M_h = \sigma_{hi}A_s a_s + \sigma_{ho}A'_s\left(h - a'_s\right) \tag{4}$$

Where A_s and $A_s^{'}$ are the cross-sectional areas of the inner and outer reinforcement cages(mm^2); a_s and $a_s^{'}$ denote the corresponding concrete cover thicknesses; h is the pipe wall thickness(mm); and σ_{vi},σ_{vo}, σ_{hi} and σ_{ho} represent the tensile stresses of the inner and outer reinforcements in the vertical and horizontal sections, respectively(MPa). These stresses are evaluated using a bilinear steel constitutive model in conjunction with strain compatibility conditions and the yield-to-failure strain limits proposed by Zhu et al. [29].

By substituting Eqs. (3) and (4) into Eq. (2), a closed-form expression for the ultimate bearing capacity of intact RCPs is obtained, which shows good agreement with full-scale TEB test data and existing design charts (average discrepancy ≈2%), and is therefore adopted as the reference bearing capacity for subsequent analyses.

(2) Residual bearing capacity of corroded RCPs

Based on the four-hinge plastic failure mechanism of a rigid ring, the bearing capacity of corroded RCPs can be regarded as a reduction of the plastic bending moments relative to intact pipes, resulting from corrosion-induced deterioration of cross-sectional geometry and material properties. Corrosion damage is mainly manifested by a reduction in the effective wall thickness due to the loss of the inner concrete cover, degradation of the yield strength and ultimate strain of the inner reinforcement caused by steel corrosion, and a weakened steel–concrete composite action [30].

$$F_c = \frac{M'_v}{R_c} + \frac{M'_i}{R_c} + 2\frac{M'_s}{R_c} \tag{5}$$

Here F_c is the residual bearing capacity of the corroded reinforced concrete pipe under the three-edge bearing condition; $M_v^{'}$,$M_i^{'}$ and $M_s^{'}$ denote the plastic bending moments at the crown, invert, and the two springline locations of the corroded pipe, respectively; and R_c is the mean radius to the centroid of the corroded cross-section, determined by the post-corrosion inner diameter and wall thickness.

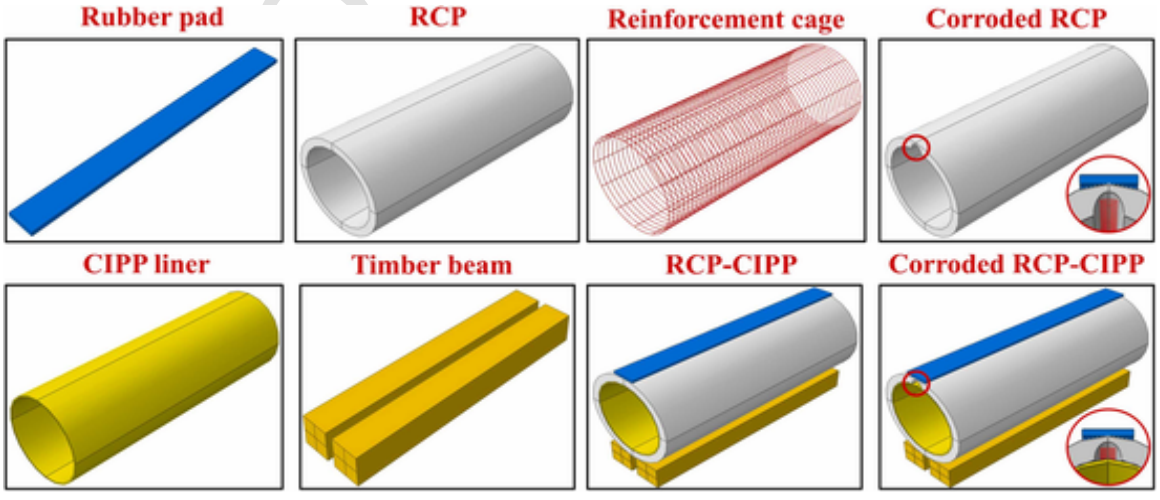

Fig. 6. Three-dimensional finite element model of the concrete pipe–CIPP liner system.

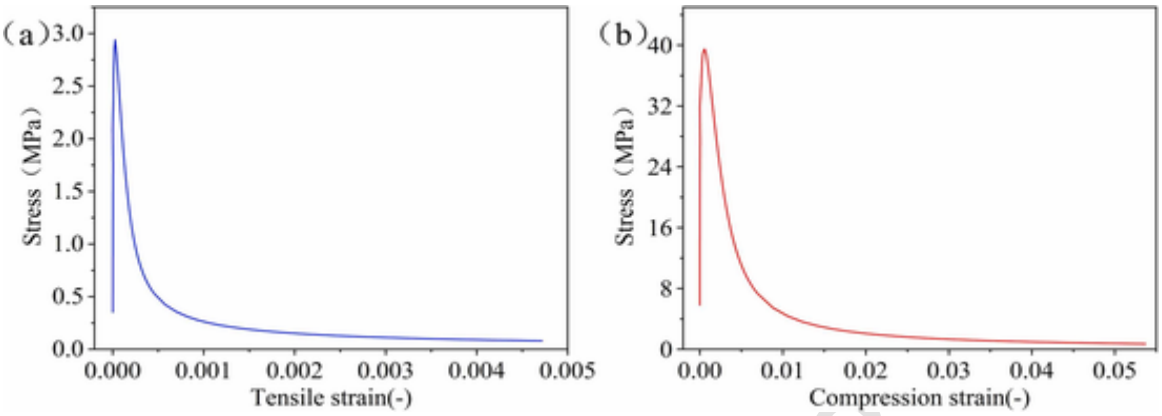

Fig. 7. Tensile and compressive stress-strain relationships adopted as constitutive inputs in the concrete damage plasticity (CDP) model: (a) tension; (b) compression.

Table 5
Parameters of the concrete damage plasticity (CDP) model.

Parameter	Dilation angle ψ	Eccentricity e	f_{b0}/f_{c0}	k_c	Viscosity parameter μ
This study	30	0.1	1.16	0.67	0.0005

Note: The CDP parameters listed in this table are commonly adopted values reported in the literature and design guidelines for normal-strength concrete [36].

For RCPs subjected to internal surface corrosion, the corrosion depth is denoted as dc. When corrosion occurs only on the inner surface, the equivalent wall thickness can be expressed as:

$$h_c = h_o - d_c \tag{6}$$

The inner diameter increases to:

$$D_c = D_o + 2d_c \tag{7}$$

Here h_o and D_o are the wall thickness and inner diameter of the intact pipe, respectively.

For the vertical sections (crown and invert), where the load-bearing mechanism is governed by the outer concrete compression zone with joint contributions from the inner and outer reinforcement cages, the post-corrosion plastic bending moment can still be expressed in the same form as that of the intact section, with material properties and lever arms evaluated using post-corrosion values, i.e.,

$$M'_v = \sigma'_{vo}A_{s,o}a'_{s,o} + \sigma'_{vi}A_{s,i}\left(h_c - a'_{s,i}\right) \tag{8}$$

Here, $a'_{s,i}$ and $a'_{s,o}$ denote the post-corrosion concrete cover thicknesses of the inner and outer reinforcement cages; and σ'_{vi} and σ'_{vo} are the tensile stresses determined based on the post-corrosion yield and ultimate states of the reinforcement. Because the plastic hinge in the vertical section primarily develops on the outer side, reduction of the inner concrete cover causes only a limited change in the corresponding lever arm.

The horizontal section (springline) is more sensitive to internal corrosion, and its post-corrosion plastic bending moment can be expressed as:

$$M'_s = \sigma'_{hi}A_{si}a''_{s,i} + \sigma'_{ho}A_{s,o}(h_c - a'_{s,o}) \tag{9}$$

Here $a'_{s,i} = a_{s,i} - d_c$, represents the effective lever arm of the inner reinforcement after corrosion-induced reduction of the concrete cover; and σ'_{hi} and σ'_{ho} are the tensile stresses of the inner and outer reinforcements, respectively, determined by considering both the loss of steel cross-sectional area and the reduction in yield strength due to corrosion.

Compared with the vertical section, the horizontal section exhibits a more pronounced reduction in bending moment due to the direct reduction of the lever arm caused by corrosion depth.

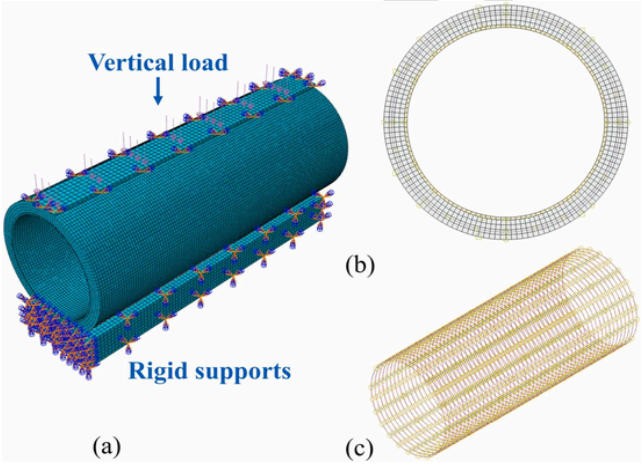

Fig. 8. Schematic of the boundary conditions and finite element model: (a) boundary conditions and loading configuration; (b) pipe-liner system; (c) reinforcing cage.

2.2. Bearing capacity modification model for RCP-CIPP composite pipes

Building upon the residual bearing capacity model for RCPs based on the plastic-hinge failure mechanism [27], this study further incorporates the strengthening effect of CIPP lining and the influence of liner thickness variation. Based on composite beam theory (Fig. 2), a bearing capacity modification model for RCP-CIPP composite structures is established.

After CIPP rehabilitation, the pipe system is approximated as a double-layer composite ring structure consisting of the original RCP and the liner. The overall bearing capacity of the composite pipe is governed by the stiffness compatibility between the concrete pipe wall and the liner, the interfacial bonding condition, and the liner thickness [31]. Assuming perfect bonding at the interface without debonding or voids, the ultimate bearing capacity of the composite pipe under the three-edge bearing condition can be expressed as:

$$F_c = F_r + \Delta F_L \tag{10}$$

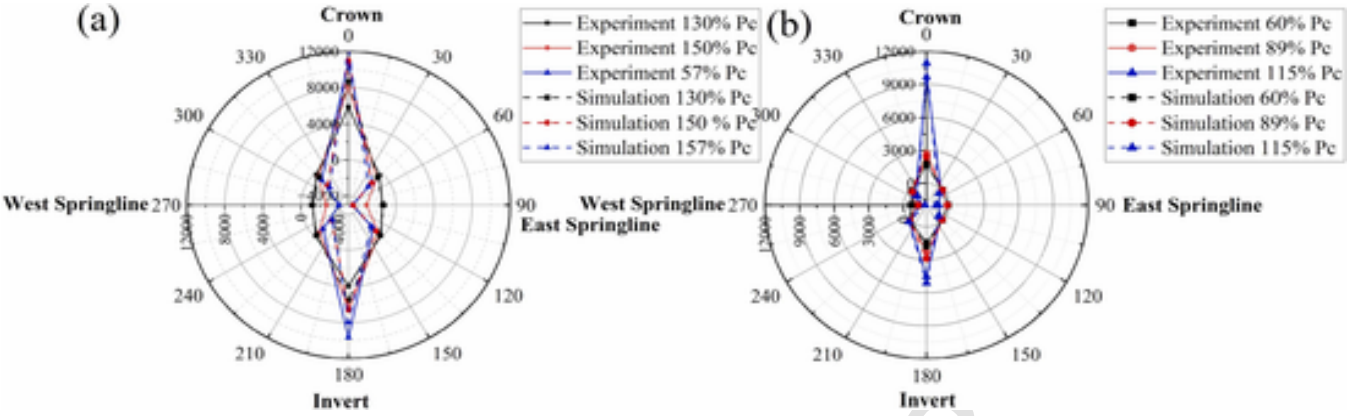

Fig. 9. Circumferential strain distribution on the inner surface of the concrete pipe: (a) RCP (b) Corroded RCP.

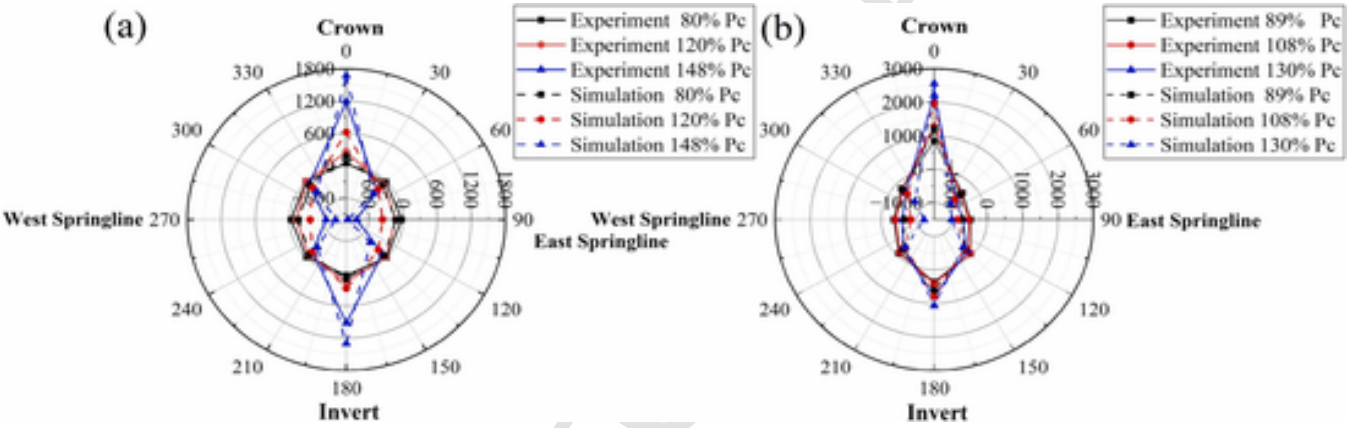

Fig. 10. Circumferential strain distribution on the inner surface of the composite pipe: (a) RCP-CIPP composite pipe; (b) Corroded RCP-CIPP composite pipe.

Here F_c is the ultimate bearing capacity of the composite pipe, F_r denotes the bearing capacity of the original RCP (intact or corroded), and ΔF_L represents the additional bearing capacity contribution provided by the CIPP liner.

The incremental bearing capacity provided by the liner primarily arises from its circumferential flexural stiffness and radial confinement effect. Based on composite beam theory, the bending moment contribution of the liner is expressed as:

$$M_L = E_L I_L \kappa = \frac{E_L t_L^3}{12(1-\mu_L^2)}\kappa \tag{11}$$

The CIPP liner is idealized as a thin-walled cylindrical shell, and its circumferential bending stiffness is evaluated using classical thin-plate theory, where EL is the elastic modulus of the liner, t_L is the liner thickness, μ_L is Poisson's ratio, and k denotes the sectional curvature. Assuming strain compatibility at the RCP-CIPP interface, i.e., $\varepsilon_L = \varepsilon_c$, the equivalent flexural stiffness of the composite section can be expressed as:

$$(EI)_{eq} = E_c I_c + n_L E_L I_L \tag{12}$$

The coefficient n_L accounts only for interfacial bonding or slip between the RCP and CIPP ($0 < n_L \leq 1$), whereas the material modulus mismatch is explicitly represented by EL and Ec. Here, E_c and I_c are the elastic modulus and moment of inertia of the concrete pipe, respectively. The interface cooperation coefficient n_L depends on the interfacial bonding condition, with $n_L = 1$ for perfect bonding and $0 < n_L \leq 1$ in the presence of interfacial slip.

According to Eq. (2), the ultimate bearing capacity modification model for the composite pipe is expressed as:

$$F_c = \frac{2}{R'}\left[M_v' + M_h' + n_L \alpha M_L\right] \tag{13}$$

The coefficient n_L governs interfacial stiffness transfer, whereas α represents the liner's effective load participation at the ultimate state. Here M_v' and M_h' are the plastic bending moments of the corroded RCP in the vertical and horizontal sections, respectively, calculated by Eqs. (8) and (9). The coefficient α is the effective participation factor of the liner in load bearing, which depends on the thickness ratio t_L/h and the degree of interfacial slip.

To quantitatively capture the strengthening effect of CIPP thickness on the composite structure, a liner thickness modification factor k_t is introduced as:

$$k_t = 1 + \beta\left(\frac{t_L}{h}\right)^{\gamma} \tag{14}$$

Here β and γ are empirical coefficients, with recommended ranges of 0.2–0.5 and 1–2, respectively, introduced to characterize the influence of the CIPP liner contribution. These coefficients are intended to be determined through subsequent numerical simulations and experimental validation.

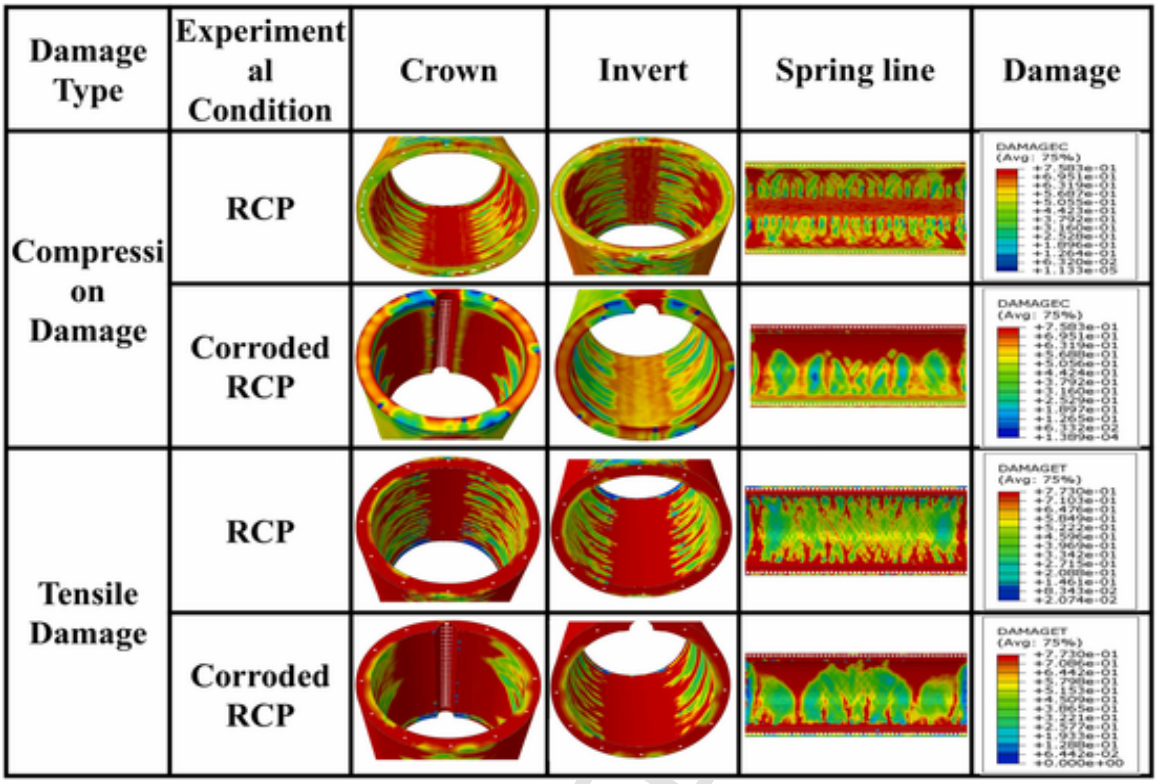

Fig. 11. Damage distribution of intact and corroded RCPs under compression and tension before rehabilitation.

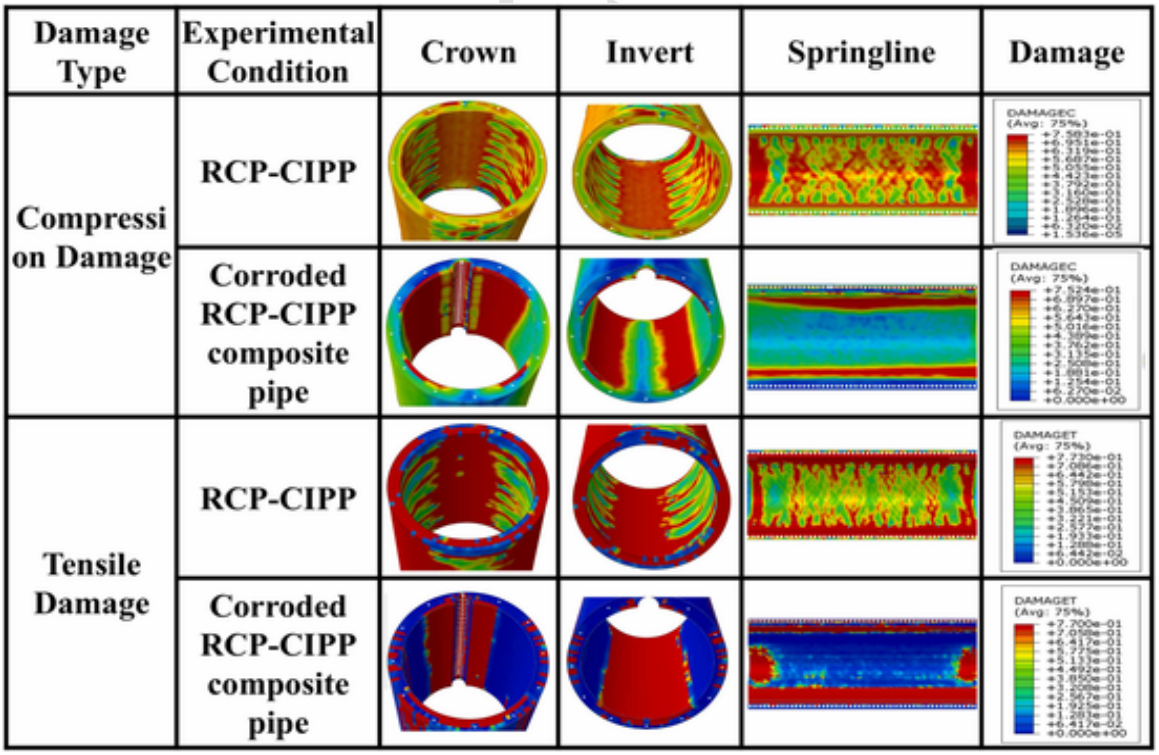

Fig. 12. Damage distribution of intact and corroded RCP-CIPP composite pipes under compression and tension after rehabilitation.

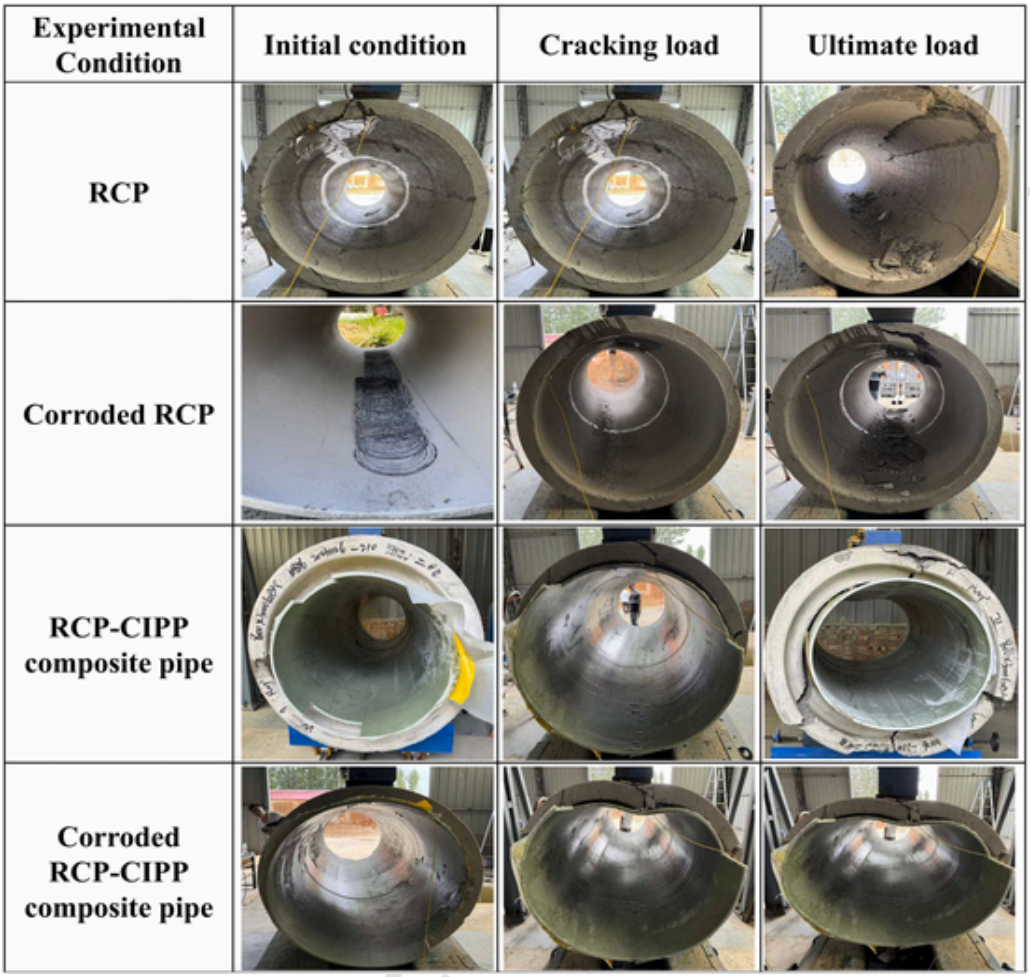

Fig. 13. Crack propagation observed in the specimens.

In summary, the ultimate bearing capacity of the RCP-CIPP composite pipe is expressed in the following unified form:

$$F_{RCP-CIPP} = k_t \cdot \frac{2}{R'} \left[M'_v + M'_h\right] \left(1 + n_L \frac{E_L I_L}{E_c I_c}\right) \quad (15)$$

The proposed expression extends the Zhu's plastic-hinge framework by incorporating liner stiffness, thickness ratio, and interfacial cooperation, enabling quantitative evaluation of the bearing capacity of RCP-CIPP composite pipes at different rehabilitation levels.

The proposed bearing capacity model is directly applied in the subsequent analysis to interpret the experimental and numerical results. The effects of liner thickness, interface interaction, and corrosion level are evaluated using Eqs. (12)-(15), and the theoretical predictions are compared with the experimental and numerical results to demonstrate the applicability of the model.

3. TEBT experimental validation

3.1. Experimental design

To systematically evaluate the strengthening effect of CIPP liners on RCPs, three-edge bearing (TEB) tests were conducted. The main objectives of the experiments were to: (i) validate the accuracy of the plastic-hinge-based Zhu model and the finite element simulations; (ii) quantitatively assess the degradation effect of pipe wall corrosion on the bearing capacity of RCPs; and (iii) investigate the strengthening mechanisms of CIPP liners with different thicknesses for both intact and corroded pipes.

Four groups of pipe specimens with different test conditions were designed in the experimental program, and the detailed grouping and basic parameters are summarized in Table 1, while the corresponding results are presented in Table 2. The RCPs were supplied as commercial precast products. The detailed concrete mix proportions were determined by the manufacturer and are not disclosed due to proprietary considerations; therefore, the concrete strength grade and experimentally measured mechanical properties are reported for structural characterization and reproducibility.

The corrosion defects were uniformly introduced at the inner surface of the pipe crown and simulated using a high-pressure water jet milling method. The dimensions of the corrosion region were controlled as 280 mm (width) × 60 mm (depth) × 2500 mm (length). The CIPP liners were fabricated using a UV-curing process, with a designed structural liner thickness of 12 mm. For each test condition, three parallel specimens were prepared to reduce experimental variability.

3.2. Experimental procedure

The experiments were conducted in accordance with the TEBT method specified in GB/T 16752–2017 [32]. The TEBT provides a standardized approach for evaluating the intrinsic structural resistance of RCPs, and its results can be related to buried pipe performance through the bedding factor.

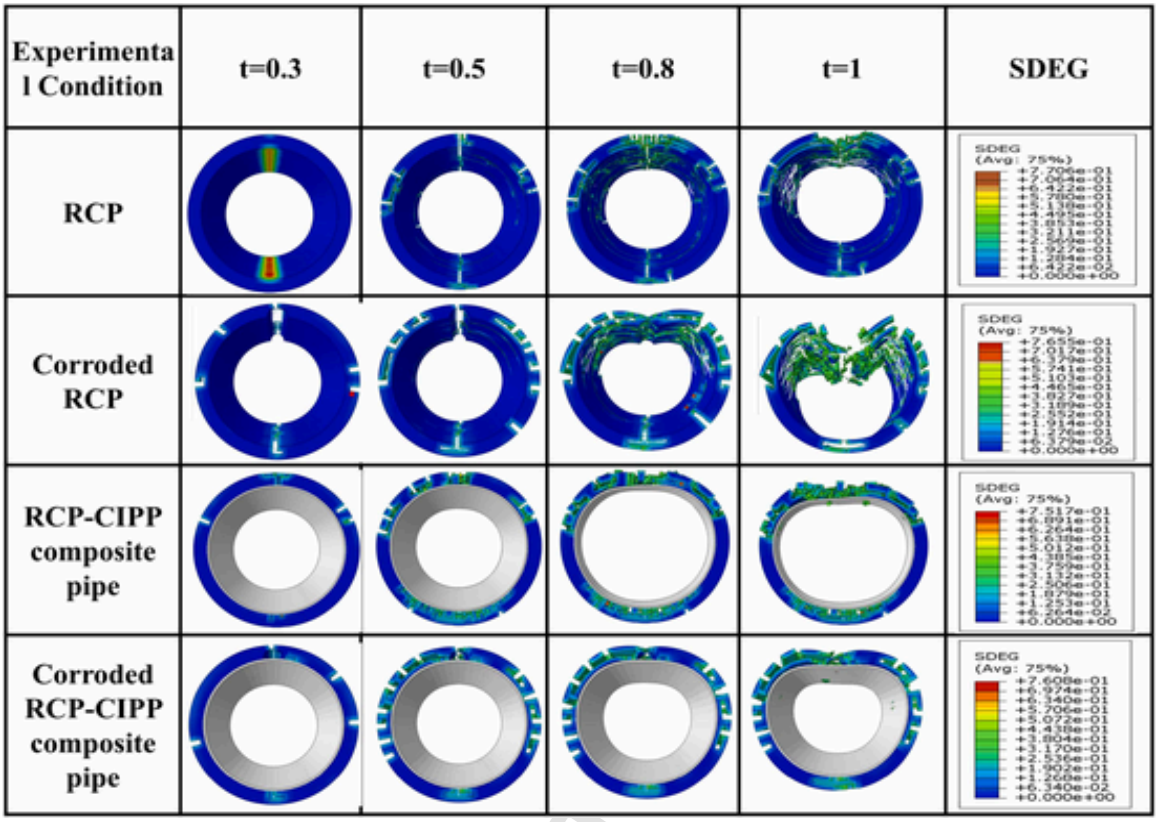

Fig. 14. Numerical simulation of the structural failure process of the pipe.

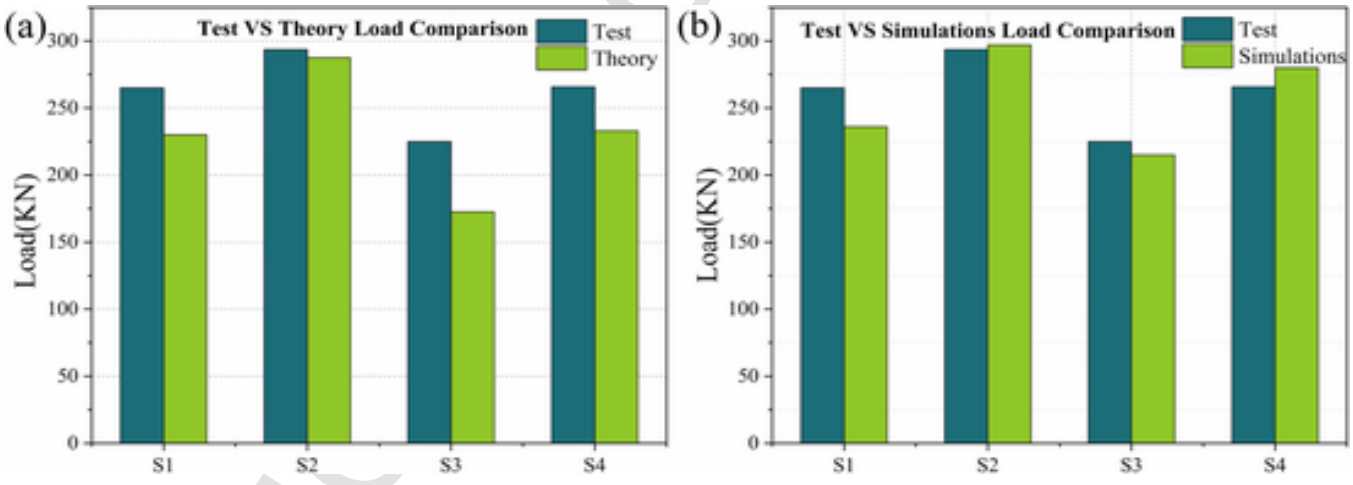

Fig. 15. Comparison of theoretical predictions, experimental results, and numerical simulations.

Specifically, the load-bearing capacity of buried pipes can be related to the load obtained from the TEBT through the bedding factor, denoted as BF, which accounts for soil support conditions. This relationship can be expressed as:

$$W_b = BF \cdot W_t \tag{16}$$

where W_b is the load required to produce the same cracking condition in the buried pipe, W_t is the load measured in the TEBT, and BF is the bedding factor reflecting soil–structure interaction effects. This approach has been widely adopted in international design standards such as AASHTO and ASCE [1,33]. Lay and Brachman [3] further confirmed that TEBT results can be directly related to buried pipe structural performance through established design relationships. Therefore, the loading method used in this study is consistent with established engineering practice. The main testing procedures are summarized as follows:

(1) Specimen installation and sensor arrangement: The pipe specimens were hoisted and positioned on the testing machine, with two parallel hardwood strips placed at the bottom as standard supports. For specimens under the corrosion condition, a corrosion region with dimensions of 280 mm × 60 mm ×

Table 6
Systematic comparison of theoretical predictions, experimental results, and numerical simulations.

Specimen	Theoretical prediction (kN)	Experimental result (kN)	Numerical simulation (kN)	Deviation (Theory–Exp) (%)
S1	260	265	258	-1.9%
S2	285	293.55	289	-2.9%
S3	220	225.07	222	-2.3%
S4	260	265.8	262	-2.2%

2500 mm was pre-formed on the inner surface at the pipe crown using a high-pressure water jet milling method. For the CIPP-rehabilitated specimens, the liner was fabricated using a UV-curing process. Distributed optical fiber sensors were circumferentially installed at a location 1 m from the inner wall of the socket end to monitor the strain distribution, as shown in Figs. 3–5.

(2) Load-controlled loading was adopted during the tests. The load was applied incrementally until failure, with predefined loading levels based on the estimated ultimate load. Each load level was maintained for a short duration to ensure a stable response. Load and strain data were synchronously recorded throughout the loading process, and crack initiation and propagation were visually observed.

4. Finite element method (FEM) evaluation

4.1. Model development

The numerical models adopted the same geometric dimensions and reinforcement configurations as the full-scale specimens. The pipe had an inner diameter of 800 mm, a wall thickness of 80 mm, and a total

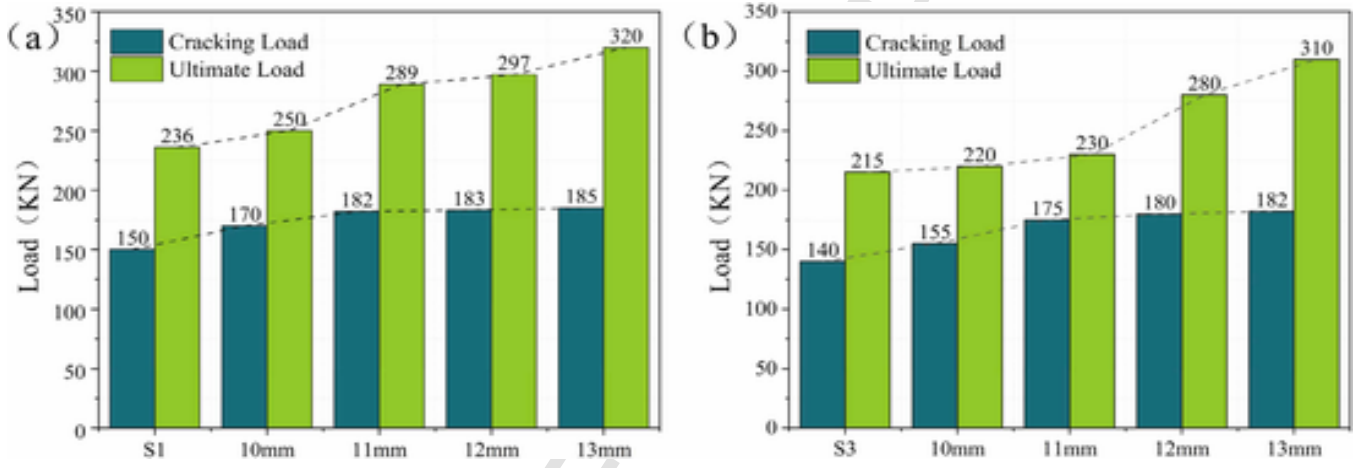

Fig. 16. Effect of liner thickness on the load-bearing performance of RCPs: (a) RCP-CIPP pipe; (b) corroded RCP-CIPP pipe.

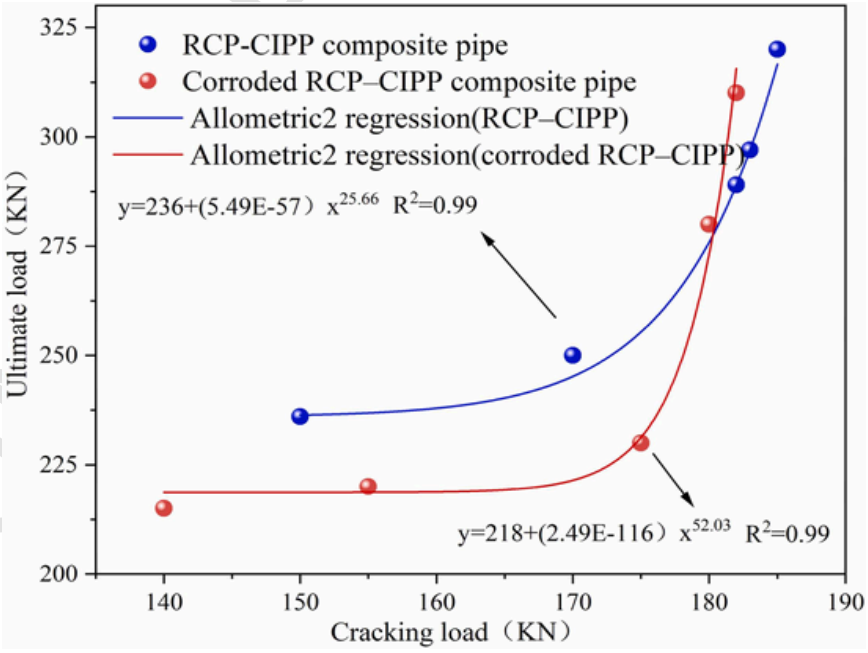

Fig. 17. Influence of cracking load on ultimate load for different liner thicknesses.

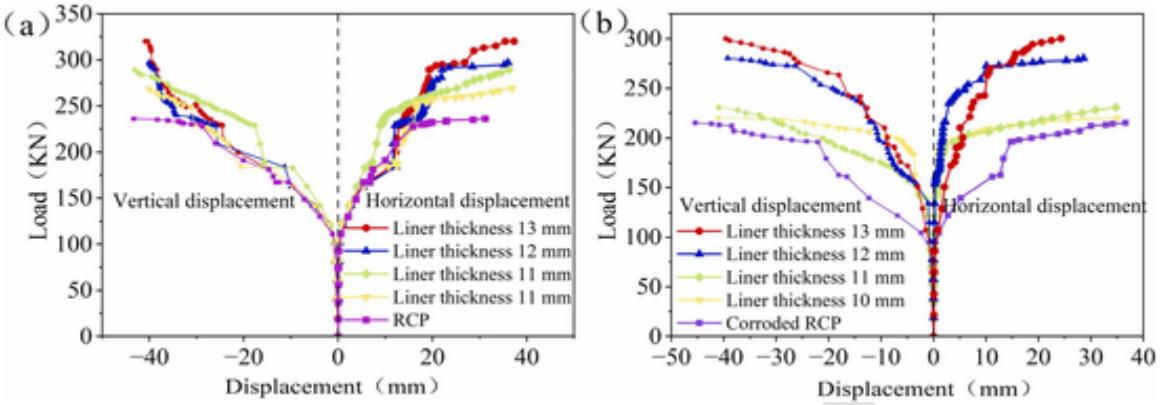

Fig. 18. Displacement responses of the composite structure before and after rehabilitation: (a) RCP-CIPP composite pipe; (b) corroded RCP-CIPP composite pipe.

length of 2500 mm. Circumferential cold-rolled steel bars were adopted as reinforcement. The bars had a nominal diameter of 5 mm and were uniformly distributed along the circumferential direction with a spacing ranging from 6 to 6.5 mm. The reinforcement layout was consistent with that used in the full-scale experimental specimens.

ABAQUS (Dassault Systèmes, Version 2024) was employed to simulate the TEBT loading of intact RCPs, corroded RCPs, and RCP-CIPP composite pipes, aiming to validate the experimental results and investigate the effect of CIPP liner thickness on the bearing capacity of composite pipes.

The finite element analysis focused on two parameters: the corrosion condition of the host pipe and the thickness of the CIPP liner. These two parameters were systematically varied in the numerical simulations, while other factors such as material properties, interface conditions, boundary constraints, and loading scheme were kept constant.

An explicit dynamic analysis step was employed in the numerical simulations. Although the TEBT represents a quasi-static loading condition, an explicit dynamic solver was adopted for numerical robustness in handling material nonlinearity, damage evolution, and contact interactions. To ensure quasi-static conditions, the loading rate was carefully controlled so that inertial effects remained negligible during the simulations, and the numerical response can therefore be regarded as quasi-static. The concrete pipe and the CIPP liner were discretized using eight-node linear reduced-integration hexahedral elements (C3D8R) with a mesh size of 20 mm, resulting in 125 elements along the pipe length of 2500 mm. The reinforcement was modeled using two-node three-dimensional linear truss elements (T3D2) and embedded into the concrete pipe using the Embedded constraint. The concrete material was described using the concrete damage plasticity (CDP) model, the steel reinforcement was modeled as an ideal elastic-perfectly plastic, and the CIPP liner was assumed to behave as a linear elastic material based on experimentally determined mechanical properties.

The material properties used in the numerical simulations, including those of concrete, steel, rubber pad, timber beam, and CIPP liner, are summarized in Table 3. These parameters were determined based on a combination of experimental testing, relevant design standards, and published literature [12,34,35].

The mechanical properties of the CIPP liner were obtained through laboratory mechanical tests. The detailed specimen preparation procedures and testing methods have been reported in our previous study [40]. The key mechanical parameters adopted in the present numerical model are summarized in Table 4, while the detailed experimental procedures and full datasets are provided in Ref. [40].

To ensure consistency with the full-scale TEBT, the numerical model was calibrated in terms of geometry, boundary conditions, material constitutive behavior, and interface interaction mechanisms. The detailed definitions of material properties, interface parameters, and boundary conditions adopted in the model are described in the following sections.

A three-dimensional finite element model was developed based on the geometry and loading configuration of the TEBT to capture the interaction between the existing pipe and the CIPP liner, as shown in Fig. 6.The model consists of the RCP (including the concrete matrix and the reinforcement cage formed by steel rebars), rubber pads,

the CIPP rehabilitation liner, and timber beams. The corrosion region is located on the inner surface at the pipe crown, consistent with the experimental configuration described in Section 3.

The reinforcement cages embedded in the reinforced concrete pipe were simulated using an ideal elastic–plastic constitutive model, while the concrete material was described by the concrete damage plasticity (CDP) model.

4.2. Concrete damage plasticity (CDP) constitutive model

The RCPs used in this study were commercial precast reinforced concrete pipes with a concrete strength grade of C45. In the numerical model, the uniaxial compressive and tensile strengths of concrete were adopted as 29.6 MPa and 2.51 MPa, respectively. The corresponding uniaxial tensile and compressive stress–strain relationships shown in Fig. 7 were adopted from relevant design standards (e.g., GB 50010–2010) and published literature [36,41]. In this model, the nonlinear behavior of concrete is characterized by isotropic elastic damage, which accounts not only for the differences between tensile and compressive responses but also for the degradation of elastic stiffness induced by tensile and compressive strains, as well as stiffness degradation induced by tensile and compressive damage [36,41].

$$\sigma_t = (1 - d_t)E_0\left(\varepsilon_t - \varepsilon_t^{pl}\right) \tag{17}$$

$$\sigma_c = (1 - d_c)E_0\left(\varepsilon_c - \varepsilon_c^{pl}\right) \tag{18}$$

Here E_0 is the initial elastic modulus of the material; σt and σc are the tensile and compressive stresses, respectively; ε_t and ε_c are the tensile and compressive strains, respectively; ε_t^{pl} and ε_c^{pl} denote the tensile and compressive plastic strains of concrete; and d_t and d_c are the uniaxial tensile and compressive damage evolution parameters of the concrete material, respectively.

The parameters of the CDP model are summarized in Table 5. These parameters are standard CDP model parameters and were adopted directly from established literature and design recommendations, rather than being treated as case-specific calibration variables.

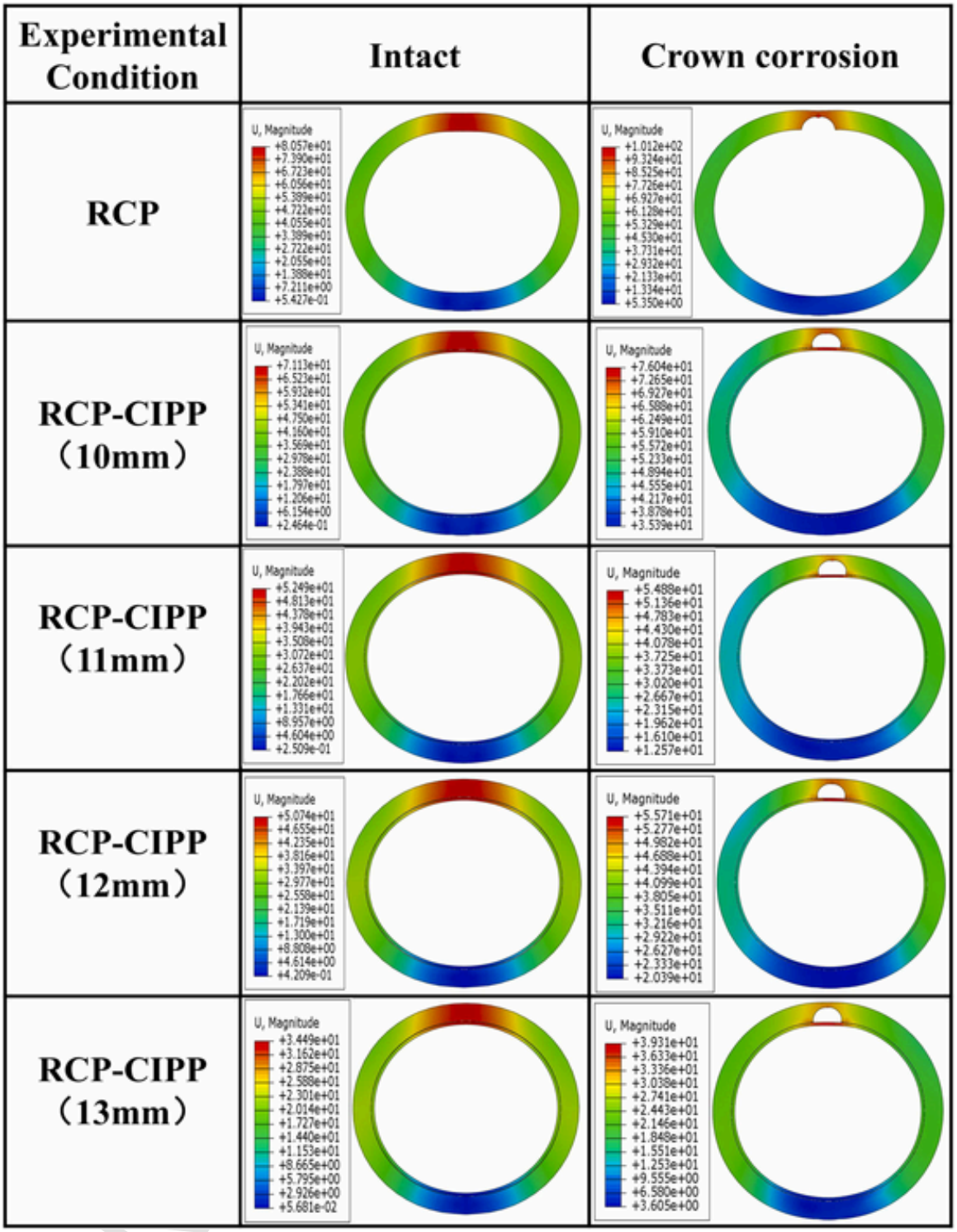

Fig. 19. Displacement contour plots of rehabilitated pipes with different liner thicknesses.

4.3. Boundary conditions and loading scheme

The existing concrete pipe rehabilitated with a UV-cured CIPP liner can be idealized as a composite beam-type structure. In accordance with composite beam assumptions, contact interactions were defined at the interface between the liner and the concrete pipe. A friction coefficient of 0.3 was assigned to the tangential behavior, while hard contact was adopted in the normal direction, following commonly reported values for concrete–polymer interfaces [42,43]. This interface treatment provides sufficient interfacial shear capacity to prevent relative slip under three-edge bearing loading conditions and represents a properly installed and fully cured liner. More complex conditions, such as debonding or installation defects, are beyond the scope of this study. Such interface imperfections may influence the local structural response and will be investigated in future work. The rubber pads were constrained in the x- and z-directions, and the lower support beams were fully fixed

to reproduce the boundary conditions of the external pressure test system (Fig. 8).

Load-controlled loading was adopted in the numerical simulations. In the experiments, the applied load was increased in a stepwise manner, with each increment equal to 10% of the cracking load Pc, until structural failure of the pipe occurred. The loading process was implemented using the *Amplitude* option in ABAQUS to control the incremental loading history.

5. Results and discussion

5.1. Comparison between numerical simulations and experimental results

To validate both the proposed analytical model and the finite element model, a systematic comparison is conducted among theoretical predictions based on Eqs. (13)–(15), experimental results, and numerical simulations. Key response parameters, including cracking load, ultimate load, and stiffness evolution, are compared in a consistent manner across the three approaches, enabling a clear and quantitative evaluation of the model accuracy and its capability to capture the structural response.

5.1.1. Circumferential strain

Circumferential strains at eight locations along the inner surface of the intact and corroded concrete pipes were extracted and plotted, as shown in Fig. 9. The intact concrete pipe exhibits a typical saddle-shaped strain distribution, with the strain magnitude increasing progressively as the applied load increases. In contrast, the corroded concrete pipe shows pronounced stress concentration and localized damage under loading, resulting in relatively large strains at lower load levels. This behavior is governed by the change in sectional stiffness and curvature demand along the pipe ring.

Corrosion reduces local stiffness and increases curvature demand, leading to strain concentration, whereas CIPP rehabilitation increases the equivalent flexural stiffness (Eq. (12)), reduces curvature, and promotes a more uniform strain distribution, particularly at the crown and invert where bending moments dominate.

The circumferential strains of the CIPP liner in the composite pipes are presented in Fig. 10. For the intact composite pipe, the strain distribution is relatively uniform, indicating that CIPP rehabilitation effectively mitigates stress concentration and promotes efficient load sharing. By contrast, the corroded composite pipe exhibits pronounced localized strain concentration, particularly in the vicinity of the corrosion region, where strain values increase markedly. This behavior indicates that corrosion-induced local strength degradation transfers higher stress demand to the CIPP liner, locally reducing rehabilitation effectiveness. Consequently, the strengthening performance of CIPP liners is strongly governed by the severity of local corrosion, highlighting the need for enhanced reinforcement in severely deteriorated regions.

The numerical results agree well with the experimental data, with differences generally within 10–15% for both intact and corroded pipes. Slight deviations at higher load levels near the corrosion region may be attributed to local material heterogeneity and idealized interface assumptions.

5.1.2. Concrete damage

Figs. 11 and 12 present the tensile and compressive damage contours of intact and corroded concrete pipes at the failure state. Under the non-corroded condition, both tensile and compressive damage levels remain relatively low, indicating limited deterioration over most regions. After CIPP rehabilitation, the overall damage level is significantly reduced, although localized damage still persists at the crown and invert, indicating enhanced resistance to external compression and improved tensile performance.

Corrosion significantly increases concrete damage, particularly at the crown and invert, due to reduced material strength. CIPP rehabilitation mitigates damage and shifts the failure mode from localized to more distributed damage. According to Eq. (13), increasing liner thickness enhances load participation and reduces stress demand at critical sections, thereby delaying hinge-controlled failure.

5.1.3. Crack development

Crack initiation and propagation observed in the experiments were well captured by the numerical simulations using the CDP model, as shown in Figs. 13 and 14. The unlined concrete pipe exhibits brittle failure with large and irregular cracks, consistent with the typical compressive behavior of concrete.

At the initial loading stage, no visible cracks or element deletion occurred. With increasing load, cracks progressively developed, accompanied by localized element distortion. Once the damage parameter reached its maximum, extensive element deletion occurred, forming large voids and indicating global structural failure. This evolution reflects progressive stiffness degradation and damage localization governed by the CDP model.

In contrast, the composite pipe exhibits a more complex failure mode with enhanced ductility. Cracks are finer and more uniformly distributed, indicating improved crack resistance and load-bearing capacity. This difference arises from a change in load transfer mechanism, where the CIPP liner provides an additional load path and redistributes tensile stresses. As a result, localized brittle cracking is transformed into a more distributed and ductile failure mode, reducing stress concentration at critical sections and delaying crack initiation and propagation.

A comparison between the experimentally observed crack patterns and the numerically predicted damage and crack evolution shows consistent crack initiation locations, propagation paths, and failure modes, confirming that the finite element model can reliably reproduce the failure behavior observed in the full-scale tests.

5.1.4. Introduction of the correction coefficient K

A comparison among the theoretical predictions, experimental results, and numerical simulations is presented in Fig. 15. Under identical test conditions, the experimental results are in good agreement with the numerical simulations, whereas the experimental values are consistently higher than the theoretical predictions. This discrepancy is mainly attributed to the simplifying assumptions adopted in the analytical model, including the idealized representation of liner contribution and section interaction.

To improve the predictive capability of the analytical model, a least-squares regression was employed to calibrate the relationship between the theoretical and experimental results, leading to the introduction of a correction coefficient, K = 1.12. With this correction, the analytical predictions show significantly improved agreement with the experimental results by compensating for the simplified assumptions in interface interaction and liner contribution.

$$K = \frac{\sum (P_{test} \cdot P_{theory})}{\sum (P_{theory}^2)} \tag{19}$$

A systematic comparison between the theoretical predictions, experimental results, and numerical simulations indicates that the proposed model is capable of reasonably capturing the load-bearing behavior of the RCP-CIPP composite system. The results are also summarized in Table 6, where the deviations between theoretical and experimental values are quantitatively evaluated.

As shown in Table 6, the corrected analytical predictions demonstrate consistently small deviations from the experimental results, with errors generally within approximately 2% for all specimens. Overall, a consistent agreement is observed among the three approaches, confirm-

ing that both the analytical model and the finite element simulations can reliably represent the structural response of the rehabilitated pipes.

5.2. Effect of CIPP liner thickness

5.2.1. Load-bearing performance

According to Eqs. (11)–(14), increasing liner thickness enhances liner stiffness and load participation, thereby increasing both cracking and ultimate loads. This reflects the increase in equivalent structural stiffness and the enhanced participation of the liner in circumferential load transfer. This trend is consistent with the validated numerical results shown in Fig. 16. For intact concrete pipes, both the cracking load and the ultimate load increase significantly with increasing liner thickness. Specifically, the cracking load increases by 13.33%, 21.33%, 22%, and 23%, respectively, while the ultimate load increases by 5.6%, 22.46%, 25.85%, and 35.59%.

For corroded concrete pipes, the introduction of a CIPP liner has a pronounced positive effect on load-bearing performance. With increasing liner thickness, the cracking load increases by 10.71%, 25.00%, 28.57%, and 30.00%, while the ultimate load increases by 2.33%, 6.98%, 30.23%, and 44.19%, respectively, compared with the unlined pipe. These results indicate that the strengthening effect of liner thickness is more pronounced in corroded pipes, because corrosion reduces the residual stiffness and load-carrying capacity of the host pipe, forcing a larger proportion of the external load to be transferred to the liner. As a result, the structural response gradually shifts from a concrete-dominated mechanism to a liner-dominated load-carrying system, particularly under severe corrosion conditions. Although corrosion substantially reduces the overall bearing capacity of the pipe, CIPP rehabilitation remains effective in enhancing both cracking and ultimate loads. Similar conclusions were reported by Islam et al. [41], who demonstrated that increasing the thickness of thermoset liners effectively improves the strength and burst capacity of pipelines.

Fig. 17 indicates a strong positive relationship between the cracking load and the ultimate load under both intact and corroded conditions. As liner thickness increases, both quantities increase accordingly, and the larger increase in ultimate load indicates that the liner contributes not only to crack delay but also to post-cracking load redistribution. Corrosion mainly reduces the magnitude of structural resistance, whereas increasing liner thickness compensates for this loss by enhancing the liner's share in circumferential load transfer.

5.2.2. Pipe displacement

Figs. 18 and 19 illustrate the displacement variations of composite pipes before and after rehabilitation for different liner thicknesses. For intact composite pipes, the displacement under the same loading condition is significantly reduced after rehabilitation, indicating that CIPP rehabilitation effectively enhances the global stiffness of the pipe.

For corroded composite pipes, the displacement variation before and after rehabilitation is more pronounced. The displacement after rehabilitation is substantially reduced, demonstrating that CIPP rehabilitation is particularly effective in reducing displacement under corrosion conditions. This reduction further indicates that the liner enhances global stiffness and suppresses deformation localization, especially in the corroded condition. This behavior can be attributed to the increase in equivalent structural stiffness and the redistribution of internal forces, which enhances global stability and reduces deformation demand under external loading.

6. Conclusions

Based on full-scale TEBT and three-dimensional finite element analyses, this study elucidates the structural behavior of corroded RCPs rehabilitated with CIPP liners and develops a design-oriented bearing capacity modification model incorporating corrosion effects and liner thickness. The main conclusions are as follows:

(1) Corrosion significantly reduces the load-bearing capacity of RCPs and must be explicitly considered in structural assessment. It mainly reduces structural resistance without altering the intrinsic cracking–ultimate load relationship governed by plastic-hinge behavior.
(2) CIPP lining provides effective structural strengthening rather than only protection, significantly improving both cracking resistance and ultimate bearing capacity of RCPs.
(3) Liner thickness is the dominant parameter governing the strengthening effectiveness of CIPP rehabilitation, particularly for deteriorated pipes. In the numerical parametric study, a 13 mm liner increases cracking and ultimate loads by 23% and 35.59% for intact RCPs and by 30% and 44.19% for corroded RCPs, indicating greater strengthening efficiency in corrosion-damaged pipelines.
(4) The developed three-dimensional finite element model accurately captures the load-bearing behavior of RCP-CIPP composite structures. Numerical predictions agree well with experimental results in terms of cracking loads, ultimate loads, and overall structural response, confirming the reliability of the modeling approach.
(5) A design-oriented bearing capacity modification model is proposed for intact, corroded, and rehabilitated RCPs. By incorporating liner thickness and corrosion effects, the model provides a unified framework for capacity evaluation. A correction coefficient calibrated using the least-squares method ($K = 1.12$) reduces prediction error to approximately 2%, demonstrating strong engineering applicability.

From a practical perspective, this study provides reference data and a design-oriented model for evaluating the load-bearing capacity of corroded RCPs rehabilitated with CIPP liners under TEBT conditions. However, the experiments were conducted under simplified loading conditions, and the numerical model involved idealized material and interface assumptions. In addition, the investigated ranges of pipe diameter, corrosion level, and liner thickness were limited. Future research should extend the analysis to buried pipeline conditions by incorporating soil–structure interaction and investigating long-term performance issues such as creep, interface degradation, and fatigue.

CRediT authorship contribution statement

Jingguo Cao: Writing – review & editing, Investigation, Funding acquisition. **Kangfu Sun:** Writing – review & editing, Supervision, Conceptualization. **Chang Ma:** Supervision, Project administration. **Jing Liu:** Writing – original draft, Resources, Methodology, Data curation. **Wenwen Du:** Validation, Investigation.

Declaration of Competing Interest

The authors declare that they have no known competing financial interests or personal relationships that could have appeared to influence the work reported in this paper.

Data Availability

Data will be made available on request.

References

[1] American Society of Civil Engineers, Standard Practice for Direct Design of Buried Precast Concrete Pipe Using Standard Installations (SIDD), American Society of Civil Engineers, Reston, VA, 2000.

[2] X. Yan, X. Wang, W. Xiang, Y. Zhao, B. Ma, Buckling behavior of Formed-in-Place-Pipe (FIPP) liners under groundwater pressure: an experimental investigation for buried municipal pipelines, Tunn. Undergr. Space Technol. 142 (2023), https://doi.org/10.1016/j.tust.2023.105397.
[3] G.R. Lay, R.W.I. Brachman, Full-scale physical testing of a buried reinforced concrete pipe under axle load, Can. Geotech. J. 51 (4) (2014) 394–408, https://doi.org/10.1139/cgj-2012-0256.
[4] B. Li, H. Fang, H. He, K. Yang, C. Chen, F. Wang, Numerical simulation and full-scale test on dynamic response of corroded concrete pipelines under multi-field coupling, Constr. Build. Mater. 200 (2019) 368–386, https://doi.org/10.1016/j.conbuildmat.2018.12.111.
[5] G. Pang, N. Wang, H. Fang, H. Liu, F. Huang, Study of damage quantification of concrete drainage pipes based on point cloud segmentation and reconstruction, Buildings (2022) 213.
[6] K. Zhai, H. Fang, N. Wang, B. Li, X. Du, K. Yang, X. Yao, Mechanical behavior of pressure pipe rehabilitated by CIPP liner under reverse fault, J. Earthq. Eng. 29 (6) (2025) 1227–1240, https://doi.org/10.1080/13632469.2025.2459786.
[7] S. Das, A. Bayat, L. Gay, M. Salimi, J. Matthews, A comprehensive review on the challenges of cured-in-place pipe (CIPP) installations, J. Water Supply. Res. Technol. - Aqua 65 (2016), https://doi.org/10.2166/aqua.2016.119.
[8] C. Wang, L. Guo, Y. Xia, C. Zhang, X. Sang, C. Xu, G. Zhu, H. Ji, P. Zhao, H. Fang, Z. Peng, X. Zhang, Flexural performance and damage evolution of multiple fiberglass-reinforced UV-CIPP composite materials-- a view from mechanics and energy release, J. Mater. Res. Technol. 29 (2024) 3317–3339, https://doi.org/10.1016/j.jmrt.2024.02.051.
[9] Y. Wu, C. Kang, M.M. Nojumi, A. Bayat, G. Bontus, Current water main rehabilitation practice using trenchless technology, Water Pract. Technol. 16 (3) (2021) 707–723, https://doi.org/10.2166/wpt.2021.026.
[10] K. Yang, H. Fang, X. Zhang, B. Li, Q. Hu, Investigation of mechanical properties of corroded concrete pipes after cured-in-place-pipe (CIPP) rehabilitation under multi-field coupling, Tunn. Undergr. Space Technol. 128 (2022), https://doi.org/10.1016/j.tust.2022.104656.
[11] B. Bosseler, D. Homann, T. Brüggemann, I. Naismith, M. Rubinato, Quality assessment of CIPP lining in sewers: crucial knowledge acquired by IKT and research gaps identified in Germany, Tunn. Undergr. Space Technol. 143 (2024), https://doi.org/10.1016/j.tust.2023.105425.
[12] ASTM International, Standard Practice for Rehabilitation of Existing Pipelines and Conduits by the Inversion and Curing of a Resin-Impregnated Tube, ASTM International, West Conshohocken, PA, 2009.
[13] W.a.W. German Association for Water, Static Calculation for Rehabilitation of Sewer Pipes and Channels with Linings and Installation Methods, German Association for Water, Wastewater and Waste (DWA), Hennef, Germany, 2015.
[14] China Association for Engineering Construction Standardization, Technical Specification for Structural Design Calculation of Buried Drainage Pipelines, China Planning Press, Beijing, 2021.
[15] X. Wang, X. Yan, S.T. Ariaratnam, B. Ma, Y. Zhao, Investigation on the load-bearing performance and interface stress of plastic pipe–CIPP liner composite Structures, Tunn. Undergr. Space Technol. 168 (2026), https://doi.org/10.1016/j.tust.2025.107160.
[16] X. Dong, T. Dou, P. Dong, Z. Wang, Y. Li, J. Ning, J. Wei, K. Li, B. Cheng, Failure experiment and calculation model for prestressed concrete cylinder pipe under three-edge bearing test using distributed fiber optic sensors, Tunn. Undergr. Space Technol. 129 (2022), https://doi.org/10.1016/j.tust.2022.104682.
[17] K. Zhai, H. Fang, D. Di, B. Li, J. Lei, M. Li, J. Ma, Mechanical behavior of the rigid pipeline strengthened by CIPP under the action of soil pressure: analytical solution and numerical simulation, Tunn. Undergr. Space Technol. 166 (2025), https://doi.org/10.1016/j.tust.2025.106938.
[18] X. Wang, C. Zeng, X. Yan, P. Zhang, Study on the bearing capacity of the polyethylene pipe–cured-in-place pipe liner composite structure under external pressure, Buildings 14 (7) (2024), https://doi.org/10.3390/buildings14072253.
[19] X. Wang, Y. Zhao, S.T. Ariaratnam, X. Yan, Study on the impact of ovality defect on structural stability of CIPP liner of drainage pipeline, Tunn. Undergr. Space Technol. 140 (2023), https://doi.org/10.1016/j.tust.2023.105338.
[20] K. Zhai, I.D. Moore, Mechanical study and equations for gravity flow pipe liners stretching across ring fractures or joints under shear action, Ocean Eng. 314 (2024) 119721, https://doi.org/10.1016/j.oceaneng.2024.119721.
[21] Z. Yahong, H. Sheng, M. Baosong, Z. Cong, Y. Xuefeng, T. Zhongsen, L. Han, D. Caiying, Experiment and evaluation model of liner design for renewal of deteriorated reinforced concrete pipes utilizing cured-in-place-pipe technology, Tunn. Undergr. Space Technol. 132 (2023) 104866, https://doi.org/10.1016/j.tust.2022.104866.
[22] ASTM International, Standard Test Methods for Concrete Pipe, Concrete Box Sections, Manhole Sections, or Tile, ASTM International, West Conshohocken, PA, 2019.
[23] American Water Works Association, Rehabilitation of Water Mains, Manual M28 ed, American Water Works Association, Denver, CO, 2014.
[24] C. He, X. Yan, B. Ma, W. Zhao, Y. Zhao, Experimental and numerical simulation of formed-in-place pipe liner for repairing water mains with void, Tunn. Undergr. Space Technol. 130 (2022) 104752, https://doi.org/10.1016/j.tust.2022.104752.
[25] L. Hu, B. Zhang, K. Yang, Numerical study on mechanical properties of corroded concrete pipes before and after cured-in-place-pipe rehabilitation 15 (11) (2023) 8586.
[26] K. Zhai, H. Fang, N. Wang, B. Li, X. Du, X. Fan, M. Du, P. Cui, X. Yao, Finite element analysis of steel pipe repaired by CIPP under fault, ce/papers 8 (2) (2025) 848–853, https://doi.org/10.1002/cepa.3174.
[27] Z. Zhu, P. Zhang, B. Ma, C. Zeng, Y. Zhao, F. Wang, Z. Li, W. Xiang, S.T. Ariaratnam, X. Yan, Quantitative model for residual bearing capacity of corroded reinforced concrete pipe based on failure mode, Tunn. Undergr. Space Technol. 129 (2022) 104675, https://doi.org/10.1016/j.tust.2022.104675.
[28] K.W. Reynolds, R.A. Loren, Structural Mechanics of Buried Pipes, CRC Press, Boca Raton, FL, 2000.
[29] K. Zhai, H. Fang, N. Wang, B. Li, X. Du, X. Fan, M. Du, P. Cui, X. Yao, A simplified solution for buried continuous pipe rehabilitated by liner under the effect of surface load and soil void, Can. Geotech. J. 62 (2025)1-15, doi:10.1139/cgj-2025-0155.
[30] K. Bhargava, A.K. Ghosh, Y. Mori, S. Ramanujam, Modeling of time to corrosion-induced cover cracking in reinforced concrete structures, Cem. Concr. Res. 35 (11) (2005) 2203–2218, https://doi.org/10.1016/j.cemconres.2005.06.007.
[31] F. Wang, J. Hua, N. Wang, S. Yan, Z. Ding, X. Xue, Effects of corrosion on bond behavior between bimetallic steel bars and seawater concrete, Constr. Build. Mater. 475 (2025) 141193, https://doi.org/10.1016/j.conbuildmat.2025.141193.
[32] Standardization Administration of China, Test Methods for Concrete and Reinforced Concrete Drainage Pipes, Standards Press of China, Beijing, 2017.
[33] American Association of State Highway and Transportation Officials, AASHTO LRFD Construction Specifications, Washington, D.C., 2010.
[34] K. Yang, J. Zhang, H. Fang, S. Ma, L. Shi, B. Li, Y. Lou, K. Yang, K. Zhai, Mechanical performances of the pipe-liner structure under void conditions, Tunn. Undergr. Space Technol. 159 (2025) 106484, https://doi.org/10.1016/j.tust.2025.106484.
[35] International Organization for Standardization, Plastics Piping Systems for the Renovation of Underground Non-Pressure Drainage and Sewerage Networks – Part 4: Cured-in-Place Pipes (CIPP, International Organization for Standardization, Geneva, 2018.
[36] Ministry of Housing and Urban-Rural Development of the People's Republic of China, Code for Design of Concrete Structures, China Architecture & Building Press, Beijing, China, 2010.
[37] X. Shen, X. Li, L. Liu, X. Chen, J. Du, Research on mechanical properties of steel-polypropylene fiber-reinforced concrete after high-temperature treatments 14 (9) (2024) 3861.
[38] A.N. Gent, Engineering with Rubber:How to Design Rubber Components, Third Edition ed, Carl Hanser Verlag GmbH & Co. KG, Munich, 2012.
[39] R.J. Ross, F.P.L. Usda Forest Service, Wood Handbook: Wood as an Engineering Material, U.S. Department of Agriculture, Forest Service, Forest Products Laboratory, 2010.
[40] J. Liu, J. Cao, C. Ma, W. Jing, K. Sun, T. Yang, Failure mechanisms and structural response of CIPP-Rehabilitated concrete pipes under external loads, Eng. Fail. Anal. 186 (2026) 110563, https://doi.org/10.1016/j.engfailanal.2026.110563.
[41] M. Islam, A. Ali, J. Alam, T. Ahmad, S. Sakib, Analysis of damage-plasticity model of concrete under uniaxial compression loading, Int. J. Eng. Technol. 10 (2021) 28–37, https://doi.org/10.14419/ijet.v10i1.30878.
[42] L. Qin, C. Guo, W. Sun, H. Guan, W. Yan, F. Wang, Experimental investigation on the interfacial shear bond performance of non-water reacting polymer and concrete, Constr. Build. Mater. 331 (2022) 127351, https://doi.org/10.1016/j.conbuildmat.2022.127351.
[43] W. Zhang, J. Lin, Y. Huang, B. Lin, X. Liu, State of the art regarding interface bond behavior between FRP and concrete based on cohesive zone model, Structures 74 (2025) 108528, https://doi.org/10.1016/j.istruc.2025.108528.